Stimulation of the human CTP:phosphoethanolamine cytidylyltransferase gene by early growth response protein 1

Lin Zhu, Christa Johnson, and Marica Bakovic[1]

Department of Human Health and Nutritional Sciences, University of Guelph, Guelph, Ontario, Canada N1G 2W1

Abstract Change in phosphoethanolamine pool size in tumor tissues is an important indicator of tumor prognosis and drug therapy efficacy. Phosphoethanolamine is the substrate of the regulatory enzyme CTP:phosphoethanolamine cytidylyltransferase (ECT) in the de novo biosynthesis of phosphatidylethanolamine (PE). Metabolic labeling with [^{14}C]ethanolamine revealed a reduced ECT activity in MCF-7 breast cancer cells, which led to an accumulation of phosphoethanolamine and a decrease in PE synthesis in comparison with MCF-10A mammary epithelial cells. The enhanced ECT activity in MCF-10A cells was due to significantly elevated CTP:phosphoethanolamine cytidylyltransferase gene (*PCYT2*) expression, at the level of promoter activity, mRNA, and protein content. The early growth response protein 1 (EGR1) could account for most of the elevated ECT activity in MCF-10A cells relative to MCF-7 cells, as evidenced by promoter-luciferase reporter assays, gel-shift analyses, and by alterations in the EGR1 gene expression. In MCF-7 cells, EGR1 is present at lower levels and the basal *PCYT2* promoter activity is maintained by proximal CAAT and GC regions and by elevated nuclear NFκB activity.▮ Together, these data demonstrate that EGR1 is an important transcriptional stimulator of the human *PCYT2* and that conditions that modify EGR1 also affect the function of ECT and consequently PE synthesis.—Zhu, L., C. Johnson, and M. Bakovic. **Stimulation of the human CTP: phosphoethanolamine cytidylyltransferase gene by early growth response protein 1.** *J. Lipid Res.* 2008. 49: 2197–2211.

Supplementary key words *PCYT2* • EGR1 • NFκB • phospholipids • phosphatidylethanolamine

Phosphatidylethanolamine (PE) is a dominant phospholipid at the protoplasmic face of all cell membranes, where it is directly involved in important cell processes such as cell signaling, membrane fusion, cell division, and apoptosis (1–4). PE can be derived from other phospholipids by decarboxylation of phosphatidylserine in mitochondria and by base-exchange mechanisms in the endoplasmic reticulum (5). However, de novo synthesis of PE through the CDP-ethanolamine Kennedy pathway is considered the most important method for contributing the majority of cellular PE and for the production of PE-plasmalogens (6). The Kennedy pathway is composed of three steps: conversion of phosphoethanolamine from ethanolamine by ethanolamine kinase (EK), formation of CDP-ethanolamine from phosphoethanolamine through the activity of CTP: phosphoethanolamine cytidylyltransferase (ECT), and combination of CDP-ethanolamine and diacylglycerol/ alkylcylglycerol to produce PE/plasmalogens (6–8).

The importance of ECT for the regulation of the Kennedy pathway has been recently reviewed (1). We established that the mouse ECT gene *Pcyt2* is regulated by alternative splicing that creates two distinct transcripts of unknown function (9). The two proteins, longer α and shorter β, differ in their catalytic properties, could form homo- and heterodimers, and could be regulated in a tissue-specific manner (10). We also produced partially deficient *Pcyt2* mice and showed that complete deletion of the mouse *Pcyt2* gene is embryonic lethal (11). These results established the essentiality of the *Pcyt2* gene and the Kennedy pathway for animal development and demonstrated that heterozygous animals maintain membrane homeostasis by downregulating PE degradation, not by stimulating phosphatidylserine decarboxylation (11).

Information on the regulation of *PCYT2* gene expression at mRNA and protein levels is scarce. Multiple metabolic and activity studies, however, suggest that the PE Kennedy pathway and ECT could be inhibited in various cancers and transformed cells, including breast cancers (1). The human ECT gene *PCYT2* is located at chromosome 17q25.3, which is in the vicinity of a tumor suppressor and is the most frequently modified region in human breast cancers and derived cell lines (9, 12). Early in cancer progression, phenotypic changes in phospholipid profiles begin and are distinguished by the elevation in phosphoethanolamine and phosphocholine contents

[1] To whom correspondence should be addressed.
e-mail: mbakovic@uoguelph.ca

(13). In breast tumor extracts and in vitro cultured cancer cells, NMR analysis demonstrated that phosphomonoester resonance signals consisted predominantly of phosphoethanolamine and phosphocholine, with their levels decreasing to normal values during either spontaneous or therapy-induced regression (13, 14). Awareness of the significance of phosphoethanolamine and phosphocholine as biochemical indicators of in vivo tumor progression and response to therapy arose more than a decade ago; however, the basic mechanisms responsible for these phenomena are not well understood.

Pcyt2 is an essential gene, and the Kennedy pathway is a ubiquitous metabolic pathway (10, 11). We are the first to isolate and characterize the human *PCYT2* promoter. The basal promoter activity was delineated by luciferase reporter assays and gel-shift analysis. The *PCYT2* promoter is driven by a functional CAAT box ($-90/-73$) and by negative ($-385/-255$) and positive ($-255/-153$) regulatory elements, demonstrating that *PCYT2* is a housekeeping gene intricately regulated by multiple transcription factors (15). The upstream promoter regions of the *PCYT2* gene could bind nuclear factor κB (NFκB) and early growth response protein 1 (EGR1), implicating their role in *PCYT2* gene regulation (15). NFκB is a heterodimeric or homodimeric complex of five distinct subunits: p65 (RelA), p68 (RelB), p75 (c-Rel), p50 (NFκB1), and p52 (NFκB2) (16). Although RelA, RelB, and c-Rel all possess C-terminal transactivation domains that drive gene transcription, p50 and p52 lack this domain and cannot activate transcription but rather act as suppressors (16). NFκB classically forms heterodimers of p65/p50 to transactivate target genes (16). EGR1 is a member of the immediate-early gene family, which also includes EGR2, EGR3, and EGR4 (17). Members of this family contain three zinc-finger DNA binding domains and, like Sp proteins, bind to GC-rich promoter regions (17). Breast cancer tissues have a greater NFκB transcriptional activity than noncancerous breast tissues (16), and there are reports suggesting that EGR1 is also aberrantly regulated in several types of cancers (18). This work aims to examine the mechanisms for the regulation of *PCYT2* gene expression in human mammary cells, and to unravel molecular mechanisms for the increase in the intracellular phosphoethanolamine pool in cancerous breast cells. We describe that changes in the expression and activity of the transcription factor EGR1 could account for the most of the *PCYT2* promoter activity and could lie behind the variations in the Kennedy pathway and PE content in human mammary cells, including breast cancer cells.

MATERIALS AND METHODS

Materials

[^{14}C]ethanolamine HCL was from American Radiolabeled Chemicals, Inc. Biotin 3′ End DNA Labeling Kit and LightShift® Chemiluminescent EMSA Kit were from Pierce. Antibodies for NFκB p65 (sc-7151), EGR1 (sc-110), Sp1 (sc-14027), Sp3 (sc-13018), and human EGR1 small interfering RNA (siRNA) (sc-29303) were all from Santa Cruz Biotechnology, Inc. ECT-specific antibodies were generated by us as initially described (11).

Cell culture

Human mammary epithelial cells (MCF-10A; American Type Culture Collection, CRL-10317™) were maintained in a 1:1 mixture of Dulbecco's modification of Eagle's and Ham's nutrient mixture F12 (DMEM/F12) supplemented with cholera toxin (100 ng/ml), epidermal growth factor (EGF) (20 ng/ml), hydrocortisone (0.5 μg/ml), bovine insulin (0.008 mg/ml), and 5% horse serum. Human breast cancer cells (MCF-7; American Type Culture Collection, HTB-22™) were maintained in MEM supplemented with 10% FBS, bovine insulin (0.008 mg/ml), 50 U/ml penicillin, and 50 μg/ml streptomycin. Cells were maintained at 37°C in a humidified 5% CO_2 atmosphere. Cell growth was assayed by 24 h cell count and protein content when no significant differences in growth rates between MCF-7 and MCF-10A cells were observed.

Radiolabeling experiments and PE content

MCF-7 and MCF-10A cells were grown until reaching 60% confluence, at which point the CDP-ethanolamine Kennedy pathway was labeled with [^{14}C]ethanolamine (0.5 μCi/dish) for 24 h. Lipids were extracted using the method of Bligh and Dyer (19). The total radioactivity from the water-methanol phase and that of the lipid phase were measured separately. [^{14}C]PE was separated from the lipid phase using TLC in a solvent consisting of methanol-chloroform-ammonia (65:35:5). Ethanolamine, phosphoethanolamine, and CDP-ethanolamine were separated from the water-methanol phase using TLC in a solution of methanol-0.5% NaCl-ammonia (50:50:5). The separated ^{14}C-labeled compounds were measured by scintillation counting. Total PE mass was determined both by gas-liquid chromatography (GLC) (Lipid Analysis, Ltd., Guelph, ON) and by TLC using the fluorescent probe 1,6-diphenylhexatriene, as we initially described (11). Lipids were extracted as above, using the method of Bligh and Dyer (19) from equal amounts of cells (1 mg protein). The lipid phase was dried with nitrogen and resuspended in 200 μl chloroform (19). One-half of the extract (100 μl) was used for GLC analysis, and the second half was separated on silica gel 60 plates (VWR) with methanol-chloroform-ammonia (65:35:5). 1,6-Diphenylhexatriene was added at 100 μM concentration, and PE was visualized by ultraviolet (UV) light excitation at 302 nm. PE mass was quantified using standard curves generated by reflection densitometry.

Enzyme assays

Cells were lysed in a homogenization buffer (10 mM Tris-HCl, pH 7.4, 1 mM EDTA, and 10 mM NaF) with protease and phosphatase inhibitor cocktails (Sigma), cell debris was removed by centrifugation (2 min at 13,000 g), and the supernatant protein content was determined with bicinchoninic acid protein assay (Pierce). EK activity was measured for 15 min at 37°C by following the phosphorylation of [^{14}C]ethanolamine (110 μCi/μmol, American Radiolabeled Chemical) with ATP as described previously (20). The reaction mixture contained 50 mM Tris-HCl buffer, pH 8.5, 10 mM ethanolamine, 7.2 μM [^{14}C]ethanolamine, 10 mM ATP, 10 mM $MgSO_4$, and cell supernatant (10.5 μg protein) in a final volume of 50 μl. Reaction mixtures were separated by TLC on silica G plates (Fisher, Canada) using the solvent system of 95% ethanol-2% NH_4OH (5:1). The radiolabeled phosphoethanolamine product was visualized by 1% ninhydrin and quantitated by liquid scintillation counting.

ECT activity was assayed using [^{14}C]phosphoethanolamine (55 μCi/μmol, American Radiolabeled Chemical) as a substrate (10). Briefly, a 50 μl mixture of 20 mM Tris-HCl buffer, pH 7.8, 10 mM MgCl$_2$, 5 mM DTT, 2 mM CTP, 10 mM unlabeled phosphoethanolamine, and 3.6 μM [^{14}C]phosphoethanolamine was incubated with cell lysates containing 15 μg protein at 37°C for 15 min. Reactions were terminated by boiling for 2 min. Reaction mixtures were then loaded onto silica G plates with CDP-ethanolamine and phosphoethanolamine standards and separated in a solvent system of methanol-0.5% NaCl-ammonia (50:50:5). Plates were then sprayed with 1% ninhydrin, and the CDP-ethanolamine product was quantitated by liquid scintillation counting.

5′-Deletion analysis

Promoter reporter constructs. The *PCYT2* promoter (AY953521) was cloned as we previously outlined in Poloumienko et al. (9). The 5′-deletion promoter constructs were prepared as we first described in Johnson, Yuan, and Bakovic (15), and they include seven clones: LUC.hET1 (−381/+53), LUC.hET2 (−252/+53), LUC.hET3 (−200/+53), LUC.hET7 (−188/+53), LUC.hET4 (−150/+53), LUC.hET5 (−42/+53), and LUC.hET6 (+6/+53). The promoter construct containing a mutated CAAT box was generated from LUC.hET1 using overlapping PCR mutagenesis to create the mutant LUChET1.CAATmut. The oligonucleotides of hET1^F 5′atttgagctcctgcactggcttccggtgtcc3′ and CAATmut^F 5′ccgagcggcgcacgcgatatcccgtgcgcag3′ were paired, respectively, with CAATmut^R 5′cacccgctgcgcacgggatatcgcgtgcgcc3′ and Glprimer2 5′ctttatgtttttggcgtcttcc3′ to produce two individual DNA fragments by PCR amplification. The two DNA fragments overlapping the region annealing with the mutated CAAT box were together used as templates for amplifying the whole length of the mutated CAAT box promoter with the primers of hET1^F and Glprimer2. The final PCR fragments were digested with the restriction enzymes and subcloned into the promoterless vector pGL3. Construct LUC.NFκBmut was generated with the same method, but using the primers of NFκBmut^F 5′ggaggtggcggcggtgatatcgtccccacgc3′ and NFκBmut^R 5′gtgcggcgtggggacgatatcaccgccgcca3′.

Luciferase assays. Approximately 3×10^6 cells were allowed to grow overnight on 60 mm plates to 60% confluence before transfection with 2.5 μg of DNA promoter-luciferase constructs and 34 ng of pRL-CMV *Renilla* vector (Promega) using 15 μg DOTAP (Avanti Polar Lipids) in serum-free media. After 5 h of incubation, the serum-free media was replaced with serum-supplemented media and the cells were cultured for an additional 42 h. Promoter activity for each of the promoter-luciferase constructs was determined using the Dual-Luciferase Reporter Assay System (Promega) and the Turner Design 20/20 Luminometer. Activity was normalized by determining the ratio of firefly luciferase activity to *Renilla* luciferase activity and was determined relative to the full-length promoter clone LUC.hET1 in MCF-7 cells.

RNA analyses

Reverse transcription and semi-quantitative PCR. Total RNA was isolated with TRIzol reagent (Invitrogen). First-strand cDNA was synthesized from 2 μg of total RNA using a poly-dT primer and Superscript II reverse transcriptase (Invitrogen). To amplify *PCYT2* and EGR1 cDNA products, PCR reactions were performed with the same amounts of single-stranded DNA of each cell line using *PCYT2*-specific primers F2 (5′acggcaggcacgggccatggg3′) and R3 (5′ctcccagcctgcttcacttcc3′), or using specific primers for EGR1 (EGR-FP: 5′ccttccccacgccgaaca3′; EGR-RP: 5′cctggggagcccgactgagtg3′). The expression of the housekeeping gene G3PDH (FP: 5′tccaccaccctgttgctgta3′; RP: 5′accacagtccatgccatcac3′) was used as a control. All PCR reactions were performed under the

following conditions: initial denaturation at 94°C for 5 min, followed by 30 cycles (23 cycles for G3PDH) of denaturation at 94°C for 30 s, 58°C annealing for 30 s, 72°C extension for 90 s, and a final extension of 10 min at 72°C. The amplified PCR products were subjected to 1.2% agarose electrophoresis.

PCYT2 mRNA stability. To establish the effect of estrogen on MCF-7 cells, MCF-7 cells were cultured for 48 h in a phenol red-free MEM containing 10% charcoal-treated FBS with or without 10 nM of 17β-estradiol. Estrogen-independent MCF-10A cells grown under regular culturing conditions were used as controls. After 48 h, all cells were treated with 1 μg/ml actinomycin D (Sigma) for 0, 1, 2, and 4 h, and at the end of each time period, total RNA was isolated and the first-strand cDNA was synthesized from 2 μg of RNA using a poly-dT primer and an 18S-RNA-specific primer (5′gagctggaattaccgcggct3′) (21). *PCYT2* cDNA was amplified as described above, and 18S-RNA cDNA, amplified with 18S-F (5′taccacatccaaggaaggcagca3′) and 18S-R (5′tggaattaccgcggctgctggca3′) primers, was used as an internal control (21).

Isolation of nuclear proteins

About 90% confluent MCF-7 and MCF-10A cells in 75 cm flasks were frozen at −80°C for 20 min and subjected to nuclear protein extraction. Cells were lysed in 0.5 ml lysis buffer (10 mM HEPES, 10 M KCl, 1.5 mM MgCl$_2$, 5% NP-40, 1 μM DTT, and protease and phophatase inhibitors), scraped into a microfuge tube, and pelleted by centrifugation at 3,000 rpm for 5 min at 4°C. After the supernatant was removed, the pellet was resuspended in lysis buffer and then centrifuged twice more before being resuspended in 40 μl extraction buffer (20 mM HEPES, 420 mM NaCl, 1.5 mM MgCl$_2$, 0.2 mM EDTA, 25% glycerol, 1 μM DTT, and protease and phophotase inhibitors) during a 10 min incubation on ice with occasional vortexing. Then nuclear debris was pelleted by centrifugation at 10,000 rpm for 5 min at 4°C, and the supernatant was diluted in a new microfuge tube with 60 μl dilution buffer (20 mM HEPES, 50 mM KCl, 0.2 mM EDTA, 20% glycerol, 1 μM DTT, and protease and phophatase inhibitors). Nuclear protein concentrations were determined using the bicinchoninic acid protein assay (Pierce), and the proteins were stored at −80°C for future use.

Electrophoretic mobility shift assays

Five double-stranded oligonucleotides covering almost the entire *PCYT2* promoter region (from −227 to −65 bp) were synthesized and used as specific probes or competitors. The sequences of the sense strand from each pair are as follows: P$_{−227/−193}$: 5′gggacagcgccccgtggaggttcccggaggtggcg3′; P$_{−191/−160}$: 5′cggtgggacggtccccacgccgcactgccccg3′; P$_{−156/−125}$: 5′gccgagcgccaggtgtgggcggtgcggagagg3′; P$_{−128/−93}$: 5′gaggccaggtgtgggtcgggggggcggggctcgggc3′; and P$_{−98/−65}$: 5′cgggccgagcggcgcacgccattggccgtgcgca3′. The 3′ end of the forward single-stranded oligonucleotide from each pair was biotinylated using the Biotin 3′End DNA Labeling Kit (Pierce). Synthetic complementary oligonucleotides were annealed at 70°C for 15 min and gradually cooled down. Electrophoretic mobility shift assays (EMSAs) were performed using the LightShift® Chemiluminescent EMSA Kit (Pierce). Binding of the nuclear extract to DNA was performed in a 20 μl reaction (2 μl 10 × binding buffer, 1.2 μg Poly(dI-dC), 2.5% glycerol, 0.05% NP-40, and 5 mM MgCl$_2$, all from the Pierce EMSA Kit. Each reaction was carried out at room temperature for 20 min using 5–10 μg of MCF-7 or MCF-10A nuclear extracts. For the competition study, 100-fold molar excess of unlabeled probe or consensus sequence for the transcription factor of interest was added prior to the labeled probe. Sequences for consensus probes were from Santa Cruz: pNFκBcon 5′agttgaggggactttcccagg3′;

pEGR1con 5′ggatccagcgggggcgagcgggggcga3′; pC/EBPcon 5′ tgcagattgcgcaatctgca3′; pNF-Ycon 5′agaccgtacgtgattggttaatctctt3′. For super-shift analysis, 0.04 μg antibody for the transcription factor of interest was used instead of its unlabeled consensus. The DNA-protein complexes were separated on a 6% polyacrylamide gel and transferred to a nylon membrane. After cross-linking under UV light for 15 min, the DNA-protein complexes were detected using HRP-conjugated streptavidin according to the manufacturer's instructions (Pierce).

Immunoblotting

The cytoplasmic and nuclear proteins were isolated from MCF-7 and MCF-10A cells and were separated on a 10% SDS-PAGE gel and transferred to a polyvinylidene difluoride (PVDF) membrane. The PCYT2, EGR1, Sp1, Sp3, and NFkB proteins were probed with specific antibodies using standard Western blotting procedures. The PVDF membranes were blocked with 5% nonfat milk in TBS-T (20 mM Tris-HCl, pH 7.5, 500 mM NaCl, 0.05% Tween-20) at room temperature for 1 h and then incubated overnight at 4°C with the primary antibody of interest (1:1000). The membranes were then washed three to four times with TBS buffer, incubated for 1 h at room temperature with the corresponding secondary antibody (1: 20,000) linked to HRP, and then visualized with enhanced chemiluminescence (Sigma).

SiRNA-mediated gene silencing of EGR1

For each transfection, 1.5 μg of EGR1 siRNA duplex (Santa Cruz) was incubated with 6 μl of transfection reagent in 200 μl transfection medium for 35 min at room temperature. As suggested by the manufacturer, 50% confluent MCF-10A cells in 6-well plates were washed twice with transfection medium and immediately transfected with the siRNA mix. Transfection of the same amount of control siRNA duplex (Santa Cruz), which contains a scrambled sequence that will not lead to the specific degradation of any known cellular mRNA, was used as a negative control. After 18 h, the transfection medium was replaced and the cells were allowed to grow for an additional 24 h in normal medium. Then cells were either collected for total RNA isolation or harvested in a homogenization buffer (9) for immunoblotting and enzyme assays.

Statistical analysis

All measurements are expressed as means from at least three independent experiments ± SD. Statistical analysis was performed using GraphPad Prism software (GraphPad, Inc.). Data were subjected to two-way ANOVA or Student's t-test, as appropriate, and differences were considered statistically significant at ***$P < 0.001$, **$P < 0.01$, and *$P < 0.05$. Densitometry analyses for the quantification of total PE mass, mRNA, and Western blotting were performed by Scion Image software (Scion, Inc.).

RESULTS

Regulation of CDP-ethanolamine Kennedy pathway in MCF-7 and MCF-10A cells

To understand the mechanisms behind the modified phosphoethanolamine pool in cancer cells, we radiolabeled both MCF-7 human breast cancer and MCF-10A normal mammary epithelial cells with [^{14}C]ethanolamine for 24 h, and measured radiolabeled precursors of the CDP-ethanolamine Kennedy pathway. Total radiolabeling of both cell types was similar, with 5,900 pmol/μg protein

in MCF-7 cells and 5,300 pmol/μg protein in MCF-10A cells (**Fig. 1A**). However, the distribution of the radiolabels was different, and the radiolabeling of water-soluble metabolites, which represents the sum of [^{14}C]ethanolamine, [^{14}C]phosphoethanolamine, and [^{14}C]CDP-ethanolamine, was ~75% of the total radioactivity in MCF-7 cells and only ~25.5% of the total in MCF-10A cells ($P < 0.05$). In line with this, the lipid-phase labeling, representing primarily PE, was ~25% of the total radioactivity in MCF-7 and ~74.5% in MCF-10A cells (Fig. 1A). We next determined the content of each water-soluble precursor and found that contributions of [^{14}C]ethanolamine, [^{14}C]phosphoethanolamine, and [^{14}C]CDP-ethanolamine were also dramatically different in the two cell lines. In MCF-7 cells, ~45% of water-soluble metabolite labeling was in the form of [^{14}C]phosphoethanolamine, whereas in MCF-10A cells, ~42% of the labeling was in the form of [^{14}C]CDP-ethanolamine (Fig. 1B). The ratio of [^{14}C]phosphoethanolamine (ECT substrate) to [^{14}C]CDP-ethanolamine (ECT product) in MCF-7 cells was 4.5 and in MCF-10A cells was 0.057 ($P = 0.000026$; Fig. 1C), indicating that the ECT activity catalyzing the CDP-ethanolamine formation is dramatically suppressed in MCF-7 cells in comparison with MCF-10A cells. At the same time, in MCF-10A cells, [^{14}C]PE in the lipid phase was 3,118 pmol/μg protein, or ~3-fold of the [^{14}C]PE present in MCF-7 cells (1,211 pmol/μg protein; $P = 0.004$) (Fig. 1D). To further address the reason for the observed changes in the phosphoethanolamine and PE pools in the two cell lines, we also measured the EK and ECT activities and quantified the total PE mass. EK activity was similar in MCF-7 and MCF-10A cells (76.8 ± 5.8 vs. 81.1 ± 5.1 mmol/mg/min), whereas ECT activity in MCF-10A cells (17.8 ± 1.1 mmol/mg/min) was ~3-fold ($P < 0.01$) higher than in MCF-7 cells (6.4 ± 0.6 mmol/mg/min). In MCF-10A cells, total PE mass was 59.7 μg/mg protein and 2-fold the PE present in MCF-7 cells (29.1 μg/mg protein; $P < 0.01$). Taken together, these data strongly suggest that the increased phosphoethanolamine pool in MCF-7 cells could be attributed to its slow conversion into CDP-ethanolamine catalyzed by ECT, not to an increased EK activity.

We postulated that the reduced ECT activity observed in MCF-7 cells relative to MCF-10A cells could be due to differences in *PCYT2* gene expression, which was tested at the level of promoter activity and mRNA and protein content as shown in **Fig. 2**. The full-length *PCYT2* promoter-luciferase construct LUC.hET1 was transfected into both cell lines (Fig. 2A), and the promoter activity was determined by luciferase reporter assays under identical conditions. As expected, the LUC.hET1 reporter had ~2.4-fold higher activity in MCF-10A cells than in MCF-7 cells ($P = 0.0045$). The *PCYT2* mRNA level in MCF-10A cells was ~2.8-fold higher than in MCF-7 cells (Fig. 2B), whereas *PCYT2* protein amounts increased ~10-fold in MCF-10A cells compared with MCF-7 cells (Fig. 2C).

Both cell lines are normally grown in the presence of estrogen-containing serum. The MCF-7 cell line, however, is an estrogen-responsive tumor cell line and increases its proliferative rate upon treatments with 17β-estradiol (E2).
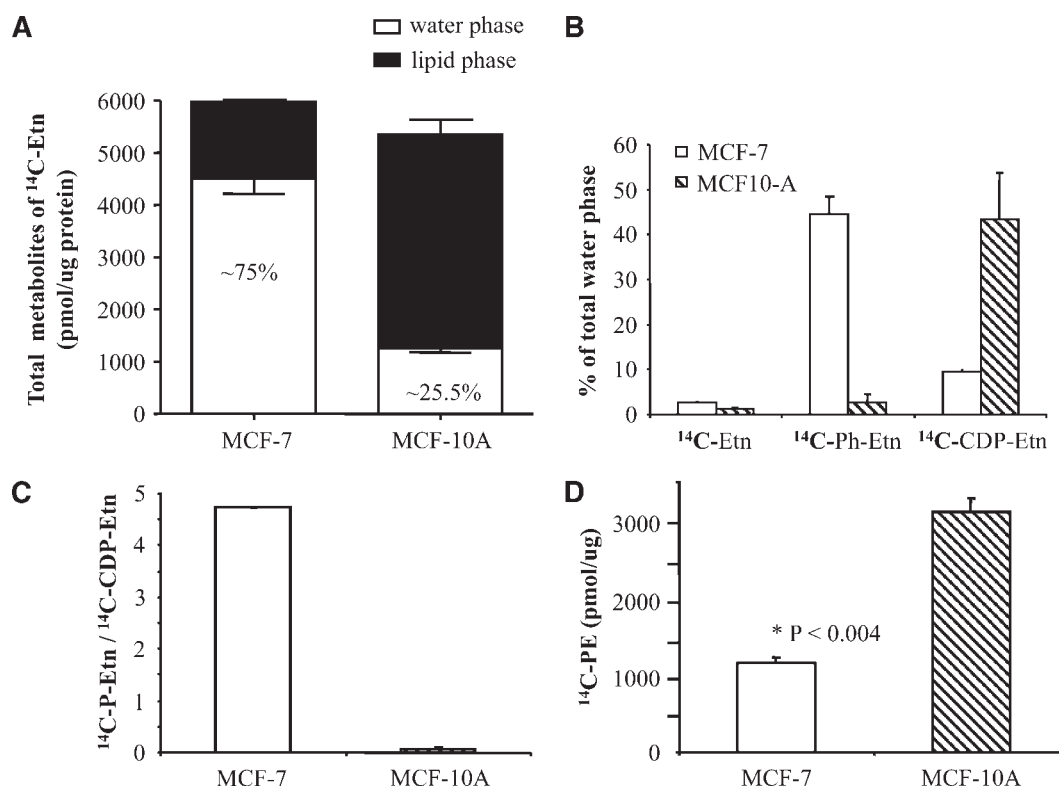
Fig. 1. Radiolabeling of the ethanolamine-Kennedy pathway. MCF-7 and MCF-10A cells grown to 60% confluency were radiolabeled with [^{14}C]ethanolamine for 24 h. A: The total radiolabeling was the same, but water-soluble and lipid-phase labeling differed between the two cell lines. Values are expressed in pmol/μg and as percent of total ^{14}C radioactivity. B: The content and distribution of ^{14}C-radiolabeled ethanolamine (Etn), phosphoethanolamine (Ph-Etn), and CDP-ethanolamine (CDP-Etn) differed in the two cell lines. C: The ratio of [^{14}C]P-Etn (ECT substrate) to [^{14}C]CDP-Etn (ECT product) is dramatically high in cancer cells. D: MCF-7 cells produce less [^{14}C]PE than do MCF-10A cells. Results are means ± SD from three separate experiments performed in duplicate.

In order to evaluate the stability of *PCYT2* message in the two cell lines and to determine how estrogen could contribute to the *PCYT2* mRNA stability in MCF-7 cells, the decay rate of *PCYT2* mRNA was assayed as shown in Fig. 2D. Overall, the *PCYT2* mRNA decayed slowly (was much more stable) in nontumorigenic, estrogen-independent MCF-10A cells than in tumorigenic, estrogen-dependent MCF-7 cells. In addition, MCF-7 *PCYT2* mRNA was more stable in the presence than in the absence of E2. Therefore, these data demonstrate that differences in the *PCYT2* mRNA stability could also contribute to the observed differences in the *PCYT2* mRNA and protein contents in the two cell lines, shown in Fig. 2B, C.

Identification of regulatory regions within the *PCYT2* promoter

To understand the mechanisms behind the transcriptional regulation of the *PCYT2* gene, we characterized the *PCYT2* promoter function in more detail. Results of the promoter 5′-deletion analysis using a series of luciferase reporter constructs identified several promoter regions responsible for the *PCYT2* regulation in MCF-10A and MCF-7 cells (**Fig. 3**). To accomplish this type of analysis, the data were first adjusted for the differences in the trans-

fection efficiencies and then expressed relative to the activity of the longest promoter construct, LUC.hET1 (−385/+53) in MCF-7 cells. In MCF-7 cells, the 5′ deletion of 130 bp to form LUC.hET2 (−255/+53) from the full-length promoter LUC.hET1 (−385/+53) resulted in 1.8-fold (*P* < 0.001) enhanced promoter activity. Additional deletions of 52 bp (−203/+53; LUC.hET3), 64 bp (−191/+53; LUC.hET7), and 102 bp (−153/+53; LUC.hET4) resulted in sequential declines in the promoter activities, all at significant levels, except for the region between LUC.hET7 and LUC.hET4 (−191 to −153 bp, Fig. 3A). In MCF-10A cells, the trends were similar, yet the promoter activity remained constantly elevated (2- to 3-fold) relative to the MCF-7 cells. In addition, a dramatically higher activity for the construct LUC.hET4 (−153/+53 bp) was obtained in MCF10A cells than in MCF-7 cells. Together, these results uncovered the presence of two upstream positive regulatory regions (−255/−203 bp and −191/−153 bp), which were only distinctive in MCF-7 cells, and one downstream region (153/+53 bp), which was the most important for the elevated activity in the MCF-10A cells (Fig. 3A). The upstream regions contained two NFκB binding sites, one at −255/−203 bp and one overlapping with EGR at −191/−153 bp. Downstream deletions from
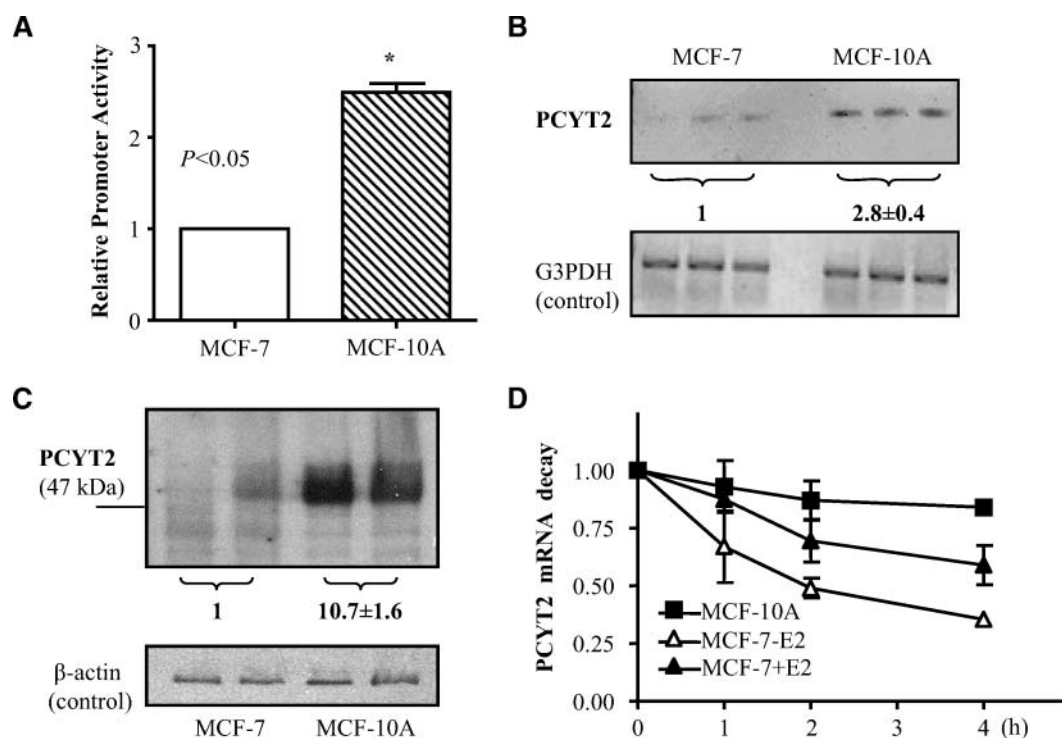
Fig. 2. Expression of *PCYT2* in MCF-7 and MCF-10A cells. A: *PCYT2* promoter activity is lower in MCF-7 cells than in MCF-10A cells. Luciferase activity of the full-length *PCYT2* promoter (LUChET1 $-385/+53$ bp) was corrected for the transfection efficiency and expressed relative to the activity in the MCF-7 cells, which was set at 1. *$P < 0.05$ from three independent experiments performed in duplicate. B: *PCYT2* mRNA levels were lower in MCF-7 cells than in MCF-10A cells. The cDNA of the housekeeping gene G3PDH was amplified as an internal control. Lanes represent three repeats of the same experiment, and numbers are mean $\pm$ SD of three independent experiments. C: *PCYT2* protein mass is lower in MCF-7 cells than in MCF-10A cells. Immunoblotting was conducted with 15 µg of protein using *PCYT2*-specific antibody and anti-β-actin as a control for the protein loading. Lanes represent two repeats of the same cell type, and numbers are mean $\pm$ SD of three independent experiments expressed relative to MCF-7 cells. D: *PCYT2* mRNA stability in MCF-10A and MCF-7 cells treated with or without 10 nM of 17β-estradiol (E2) as described in Materials and Methods. Shown are time curves for the *PCYT2* mRNA corrected at each point by the abundance of 18S-RNA used as an internal standard in RT-PCR. Shown are mean $\pm$ SD from at least two separate experiments performed in duplicate or triplicate.
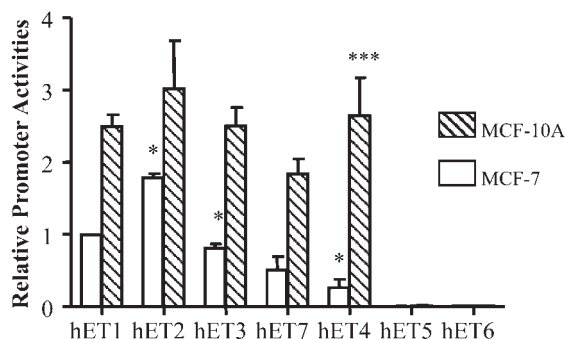
-153 to -43 bp and -43 to $+6$ bp (LUC.hET5 and LUC.hET6) completely abolished promoter activity in both cell types ($P < 0.001$), indicating that the promoter region from -153 to -43 bp contains elements for the basal promoter activity. The main elements within this region are parts of the LUC.hET4 ($-153/+53$ bp), also the most distinctive area for the differences between the two cell lines, and they include one CAAT box and two GC-rich regions for Sp and EGR transcription factors. These important regions are shown in Fig. 3B, and their separate functions will be examined in more detail in the following sections.

The importance of the CAAT box ($-82/-71$ bp) for the basal *PCYT2* transcription

We previously established (15) that the *PCYT2* promoter is a TATA-less promoter that has a functional CAAT box at position -82 bp to -71 bp upstream from the transcription start site, which is critical for the basal transcriptional activity of *PCYT2*. Using a gel shift analysis with a probe from the same region (P$_{-98/-65}$ in Fig. 3B), we confirmed

that P$_{-98/-65}$ specifically binds NF-Y and EGR transcription factors in human mammary cells (**Fig. 4A**). The binding was completely abolished by 100-fold molar excess of P$_{-98/-65}$ NF-Y and EGR consensus sequences but not by C/EBP consensus. To further test the specific role of the CAAT box in *PCYT2* transcription, we mutated the CAAT box sequence CATTGG $\rightarrow$ GATATC within the full-length promoter-luciferase reporter ($-385/+53$, LUC.hET1) and performed luciferase assays in both MCF-7 and MCF-10A cells (Fig. 4B). The luciferase reporter assays showed that this mutation reduced the promoter activity to 20–40% in both cell lines, demonstrating that *PCYT2* transcription strongly depends on a fully functional CAAT box that is not cell-type specific. Therefore, the significant decline in the *PCYT2* promoter activity in the MCF-7 cells and constantly elevated activity in the MCF-10A cells observed after deletion of a broader promoter region ($-153/-43$ bp; Fig. 3) appear to be the results of different types of regulation produced by interactions of distinct upstream promoter enhancers with the core CAAT binding proteins. Described below are experiments performed to

A 5'-Deletion Analysis

Relative Promoter Activities

MCF-10A
MCF-7

hET1 hET2 hET3 hET7 hET4 hET5 hET6

B *PCYT2* Promoter Structure

P₋₂₂₇/₋₁₉₃ P₋₁₉₁/₋₁₆₀ P₋₁₅₆/₋₁₂₅ P₋₁₂₈/₋₉₃ P₋₉₈/₋₆₅

+53

LUC

-385   -255   -203   -191   -153   -43   +6
hET1   hET2   hET3   hET7   hET4   hET5 hET6
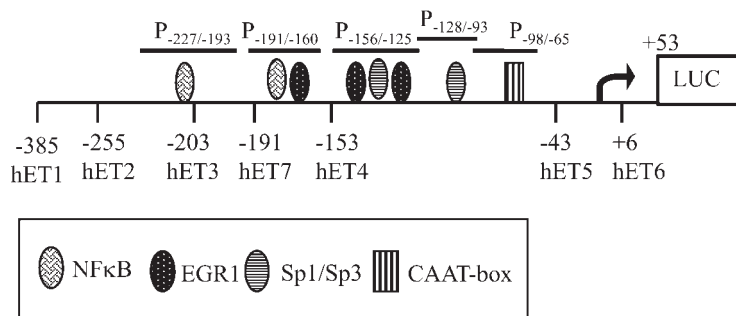
NFκB   EGR1   Sp1/Sp3   CAAT-box

Fig. 3. Identification of the *PCYT2* promoter regulatory regions. A: 5′-Deletion analysis of the *PCYT2* promoter-luciferase reporters in MCF-7 and MCF-10A cells. Luciferase activities were measured 48 h after transfection and corrected for the transfection efficiency by the *Renilla* luciferase reporter as described in Materials and Methods. The corrected activities were then expressed relative to the activity of the full-length construct LUChET1 (−385/+53 bp) in the MCF-7 cells, which was set at 1. Values are mean ± SD from at least three independent duplicate experiments. *P < 0.05 for hET1 vs. hET2, hET3 vs. hET2, and hET4 vs. hET3. ***P < 0.001. B: Schematic representation of the 5′-deletion strategy for the luciferase constructs hET1-hET7 also showing the position and the organization of transcription factor binding sites analyzed by site-directed mutagenesis and electrophoretic mobility shift assays (EMSAs). The location of five promoter probes used in EMSAs is shown at top.

delineate this distinct cell type-dependent regulation of the *PCYT2* promoter function.

Roles of two GC boxes and EGR1 for stimulated gene transcription in MCF-10A cells

Promoter deletion analysis showed that the construct LUC.hET4 (−153/+53) processed 10-fold higher (0.26 vs. 2.65; *P* < 0.01) luciferase activity in MCF-10A cells than in MCF-7 cells, whereas LUC.hET5 and LUC.hET6 (−43/+53 bp and +6/+53 bp, respectively) completely lost activity in both cell types (Fig. 3A). This implies that the transcription factors responsible for the enhanced activity in MCF-10A cells are located between −153 and −43 bp. To test which transcription factors are responsible for this regulation, two probes covering two GC-rich regions, P₋₁₅₆/₋₁₂₅ and P₋₁₂₈/₋₉₃, were designed for EMSA (**Fig. 5**). Both probes contain putative binding sites for EGR1 and Sp transcriptional factors. EMSA analysis demonstrates that nuclear extract from MCF-10A cells formed three specific complexes with the more upstream probe, P₋₁₅₆/₋₁₂₅ (Fig. 5A). The complex shown as band *b* represents Sp1-EGR1 DNA interaction, because this band was shifted by 100-fold molar excess of unlabeled P₋₁₅₆/₋₁₂₅ and Sp and EGR consensus, and super-shifted by Sp1 and EGR1 antibodies. Similarly, band *c* represents a mix of Sp3 and EGR DNA complexes, because band *c* could be competed for by 100-fold molar excess of "cold" P₋₁₅₆/₋₁₂₅ probe, Sp3 and EGR1 antibodies, and by both Sp3 and EGR consensus sequences. Band *d* is indicated as EGR1/Sp(?) DNA complex because the intensity of this band was reduced by an excess of unlabeled P₋₁₅₆/₋₁₂₅ and Sp and EGR consensus but super-shifted only by EGR1 antibody. Sp1- and Sp3-specific antibodies did not have an effect on band *d*,

suggesting that some other Sp subtype could be involved in this interaction (Fig. 5A).

The second GC probe, P₋₁₂₈/₋₉₃, is positioned immediately downstream of the probe P₋₁₅₆/₋₁₂₅. As shown in Fig. 5B, this region specifically interacts with Sp1 and Sp3 transcription factors, indicated as bands *e* and *f*, which were super-shifted by their specific antibodies. P₋₁₂₈/₋₉₃ is GC-rich and might also be targeted for EGR binding, as was probe P₋₁₅₆/₋₁₂₅. No effective EGR binding was detected for this region, but transcription factors Sip (band *f*) and an as-yet-unidentified Sp family member (band *g*) could be involved in the interaction with this region.

We next analyzed the cell type differences in cellular and nuclear distribution of the main GC-regulatory transcription factors, EGR1, Sp1, and Sp3 (**Fig. 6A, B**). EGR1 was abundantly present in both cytosol and nuclei of MCF-10A cells, which is in contrast to a very low presence in MCF-7 cells (Fig. 6A). Unlike EGR1, nuclear content of Sp1 and Sp3 proteins were similar in both cell types, even though their inactive cytosolic pools were significantly higher in MCF-7 cells than in MCF-10A cells (Fig. 6B). To test whether the cell-specific differences in EGR1 protein levels would affect its binding activity to the *PCYT2* promoter, we also performed EMSA using MCF-7 nuclear extracts and the probe P₋₁₅₆/₋₁₂₅. As shown in Fig. 6C, the bands *b*, *c*, and *d*, which were shifted by EGR consensus probe and anti-EGR1 antibody when MCF-10A nuclear extracts were used (Fig. 5A), could not be competed for by the EGR1 consensus probe and its specific antibody when MCF-7 nuclear extracts were used. These bands were, however, specifically competed for by Sp1/Sp3 consensus probe and specific antibodies. These data, together with the promoter activity assays (Fig. 3) and EMSA analysis (Fig. 5), strongly
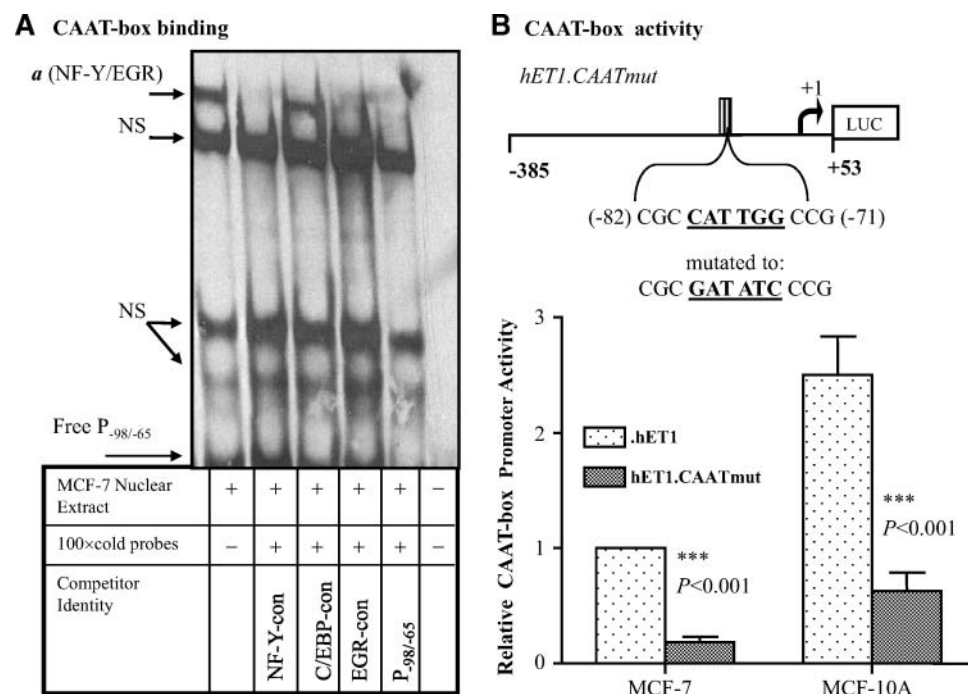
Fig. 4. The CAAT box ($-79/-74$ bp) is critical for the basal promoter activity. A: EMSA analysis for the core promoter probe $P_{-98/-65}$ and MCF-7 nuclear extracts. The single specific interaction (band *a*) was competed for by 100-fold molar excess of the "cold" probe $P_{-98/-65}$ or the consensus probes for NF-Y and early growth response protein 1 (EGR1) transcription factors. Nonspecific (NS) bindings are indicated. Shown is an autoradiograph representative of at least three individual experiments. B: Diagram of the CAAT box mutation construct LUChET1.CAATmut that was produced from the full-length promoter construct LUC.hET1 ($-385/+53$ bp) by replacing CATTGG with GATATC sequence (top). The luciferase activity of the LUChET1.CAATmut relative to the wild-type promoter construct LUC.hET1 is severely reduced in both MCF-7 and MCF-10A cells (bottom). The results shown are means $\pm$ SD from three separate experiments performed in duplicate. ***$P < 0.001$.

indicate that the transcription factor EGR1, but not Sp1 and Sp3 factors, is responsible for the upregulated *PCYT2* promoter activity and gene transcription in MCF-10A cells.

Modifications of the EGR1 gene expression

Because the elevated nuclear EGR1 in MCF-10A cells is due to the abundant protein expression, and given that EGR1 binds to several *PCYT2* promoter regions, we used siRNA-mediated gene silencing to test the effect of depleting the EGR1 content on the Pcyt2 mRNA and protein expression. Indeed, when the EGR1 gene was silenced by its specific siRNA (0.61-fold), *PCYT2* expression was dramatically reduced at the mRNA level (0.63-fold) and hardly detectable EGR1 (0.16-fold) and PCYT2 (0.07-fold) proteins were obtained by Western blotting (**Fig. 7A, B**). Under the same conditions, the ECT activity was also severely reduced by EGR1 silencing and was only 1.3 ± 0.4 mmol/mg/min or 8.3% of the activity in the siRNA control-treated cells (15.6 ± 1.9 mmol/mg/min; $P < 0.005$).

Because the EGR1 gene is responsive to a multitude of extracellular signals, including growth factors (22), insulin (23, 24), and corticosteroids (25), we cultured MCF-7 cells (express low EGR1) in the media of MCF-10A cells (express abundant EGR1, Fig. 6A), and these data are shown in Fig. 7C. The new media (DMEM/F12 containing 5% serum, EGF, hydrocortisone, and insulin) induced the expression of EGR1 in MCF-7 cells by 2.2-fold relative to the standard media (MEM containing 10% serum and insulin). The increase, however, was below the EGR1 levels detected in MCF-10A cells grown in the same media (10-fold in Fig. 6A). In parallel, *PCYT2* protein increased 4.7-fold when MCF-7 cells were switched to the DMEM/F12 media (Fig. 7C) but was below the levels in the MCF-10A cells grown under the same conditions (10.7-fold in Fig. 2C). Therefore, we concluded that in MCF-7 cells, EGR1 levels could be increased by different culture conditions that directly impact *PCYT2* gene expression, yet there are additional, inherent differences between the two cell types that contribute additional EGR1 in MCF-10A cells and therefore different regulation of *PCYT2* in these two cell lines.

Role of NFκB in *PCYT2* promoter regulation in MCF-7 cells

As demonstrated by 5′-deletion analysis for the luciferase constructs hET2-hET4 (Fig. 3A), NFκB binding sites within the promoter region $-255/-153$ bp are responsible for the *PCYT2* regulation in MCF-7 cells. In our previous characterization of the *PCYT2* promoter, we established that in HeLa cells, NFκB and EGR1 could both bind to the promoter region $-190/-160$ bp and that in addition, a second NFκB site could be present (15). Elevated NFκB activity has been seen frequently in breast cancers
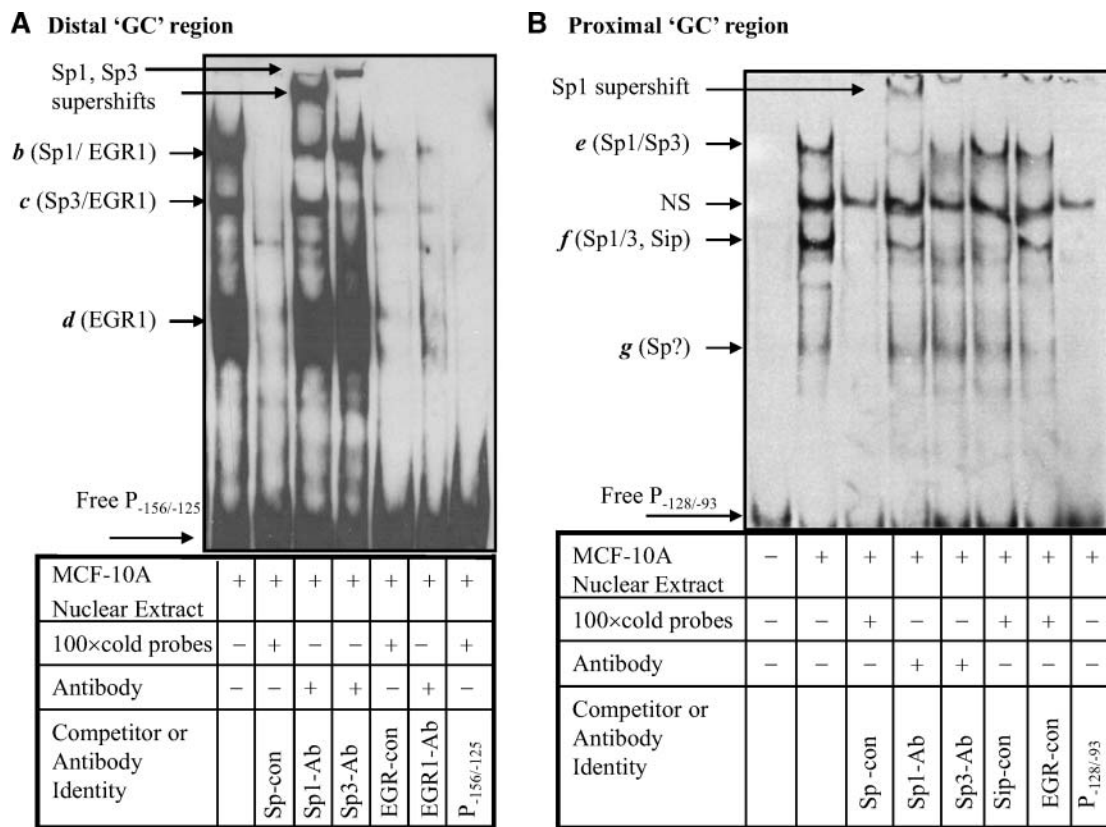
Fig. 5. EMSA of two GC-rich promoter regulatory regions. A: Gel-shift and super-shift analyses of a distal GC region using the probe $P_{-156/-125}$ and MCF-10A nuclear extracts. Specific interactions were competed for by consensus probes and antibodies to Sp1, Sp3, and EGR1 as indicated at the left of each panel. B. Gel-shift and super-shift analyses of a proximal GC region using the probe $P_{-128/-93}$. The shifted bands indicated as *e* and *f* were competed for by the excess of the "cold" $P_{-128/-93}$ probe, the consensus Sp probe, and the specific antibodies for Sp1 and Sp3 transcription factors. Band *g* was competed for by the Sp consensus but was not Sp1- and Sp3-related. Band *f* could also be interrupted by Sip. One nonspecific DNA-protein complex is also indicated.

(16). To test whether NFκB participates in the regulation of the *PCYT2* promoter in MCF-7 cells, two probes (each probe individually containing an NFκB site), together covering the entire positive regulatory region, were used for EMSA. $P_{-227/-193}$ had a single NFκB binding site at position $-212/-207$ bp, and $P_{-191/-160}$ contained an overlapping site for NFκB and EGR1 at position $-187/-182$ bp. As shown in **Fig. 8A**, $P_{-227/-193}$ formed two specific DNA-protein complexes, the stronger *h* and the weaker *i*. Both complexes were interrupted by 100-fold molar excess of specific unlabeled $P_{-227/-193}$ or NFκB consensus probe, and band *h* was eliminated by the anti-NFκBp65 antibody, whereas band *i* appeared stronger. These data indicate that band *h* represents the DNA-protein complex containing the active p65 subunit of NFκB and band *i* is most probably from an interaction with a different NFκB subunit (p50 or other).

With the probe $P_{-191/-160}$, one protein-DNA band was detected in MCF-7 cells (Fig. 8B). The formation of this complex could be interrupted by 100-fold excess of the same unlabeled probe, as well as by NFκB or EGR consensus probes (Fig. 8B). The band was also specifically competed for by antibodies to NFκB p65 and EGR1, in agreement with our previous observation that both factors could bind to this region when using HeLa nuclear extracts (15). We specifically mutated the NFκB binding site

within the $P_{-191/-160}$ region by replacing GGACG with ATATC (Fig. 8C) and performed luciferase assays in both MCF-7 and MCF-10A cells. The mutation of the NFκB site reduced the luciferase activity of the full-length promoter by ~35% in MCF-7 cells but had no significant effects in MCF-10A cells, suggesting different functional activities of NFκB in these two cell lines. NFκB p65, in its inactive state, exists in the cytosol, bound to inhibitory IκB molecules, and the activation of the pathway leads to the nuclear localization of the p65 subunit (26). Localization of NFκB in both cell lines was analyzed by immunoblotting, as shown in Fig. 8D. An abundant NFκB p65 existed in the inactive state in MCF-10A cytosol and could not be detected in its active nuclear state. In contrast, in MCF-7 cells, cytosolic NFκB p65 could not be detected, because it was present primarily in the nucleus, demonstrating that the activation of NFκB was higher in MCF-7 cells than in MCF-10A cells. The absence of nuclear NFκB protein in MCF-10A cells agrees with the mutational analysis in Fig. 8C and the 5′-deletion analysis (Fig. 3) showing that the promoter fragment ($-255/-153$ bp) containing two NFκB sites is regulatory in MCF-7 cells but not in MCF-10A cells. As we described earlier, the *PCYT2* promoter regulation in MCF-10A cells is instead strongly dependent on the EGR1 family of transcription factors.
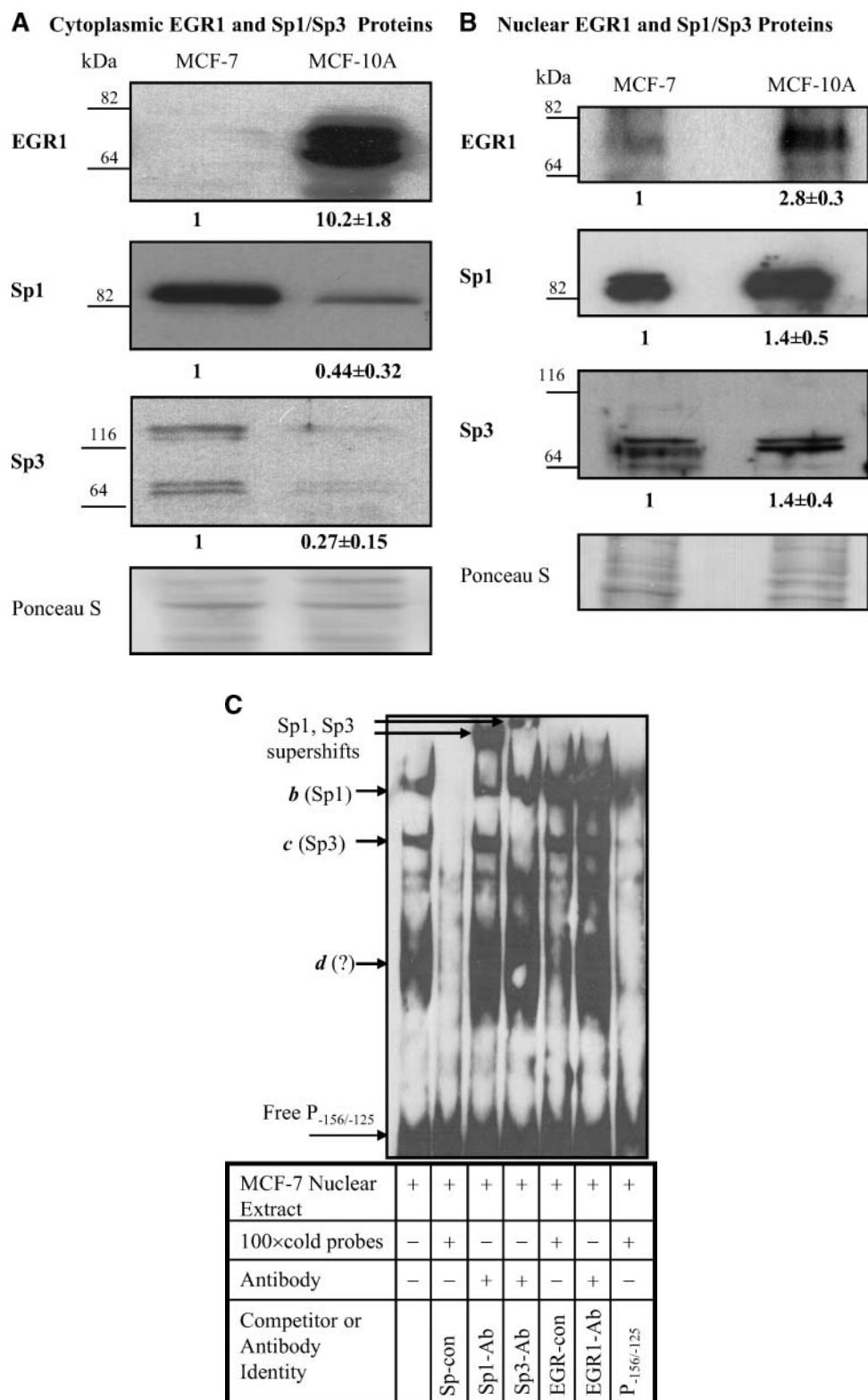
Fig. 6. Expression of the GC binding factor EGR1. Cytoplasmic (A) and nuclear (B) protein contents of EGR1, Sp1, and Sp3 were compared in MCF-10A and MCF-7 cells by Western blotting showing that ERG1 was virtually absent in MCF-7 cells and very abundant and present in active, nuclear form in MCF-10A cells. Although more expressed in the MCF-7 cytosol, nuclear Sp1 and Sp3 did not differ in both cell types. Twenty-five micrograms of proteins from each cell line were used for each Western blotting. Also included is densitometric analysis for at least three independent experiments performed in duplicate and quantified as mean $\pm$ SD relative to the values in MCF-7 cells. C: EMSA using the probe $P_{-156/-125}$ and MCF-7 nuclear extracts. The bands b, c, and d correspond to those seen in Fig. 5A. Shown is an autoradiograph representative of three separate experiments.
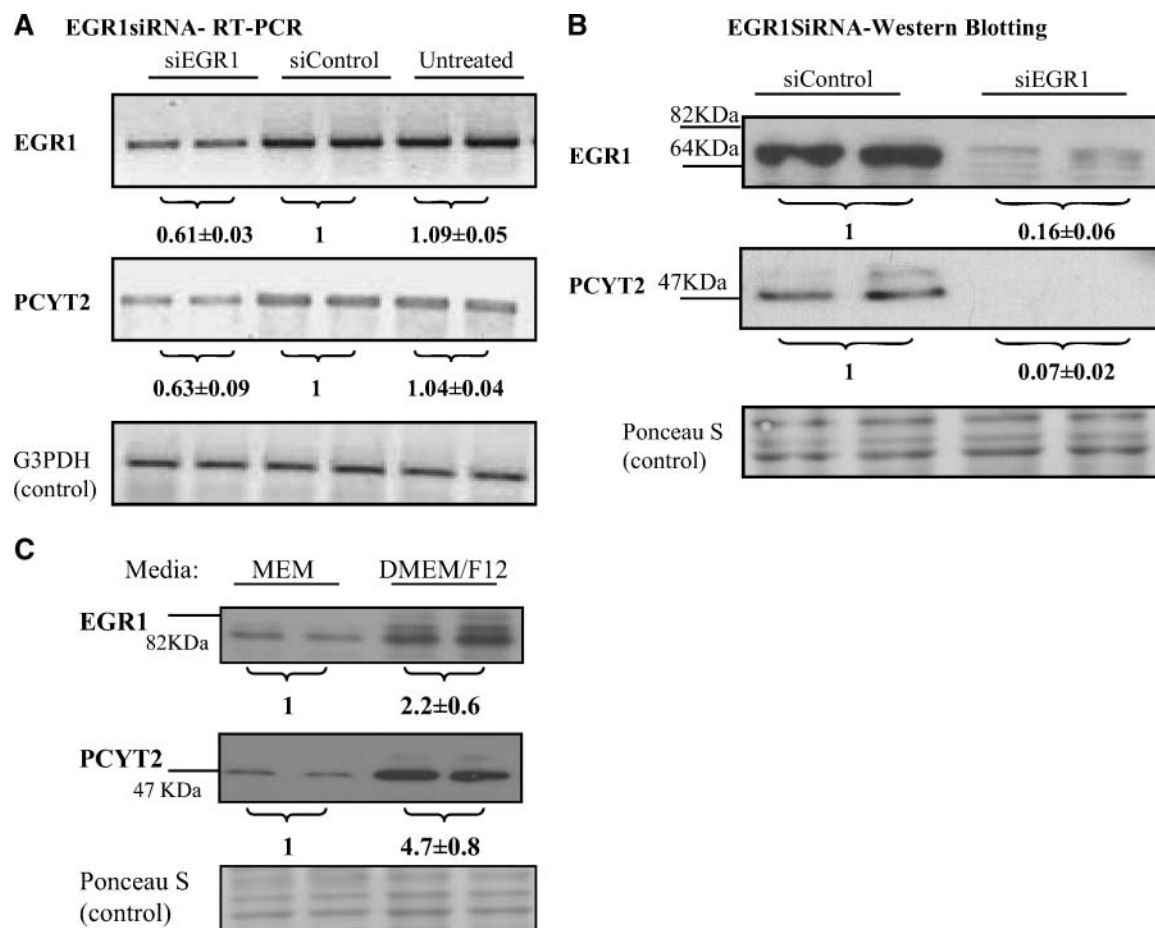
Fig. 7. Identification of the role of EGR1 in *PCYT2* expression. A: The content of both *PCYT2* and EGR1 mRNA in MCF-10A cells transfected with EGR1-specific small interfering RNA (siRNA) was vividly reduced relative to the transfections with a control siRNA duplex (siControl) or untransfected cells. The housekeeping gene G3PDH was amplified as an internal mRNA control. Numerical data represent EGR1/G3PDH and Pcyt2/G3PDH ratios from three separate experiments, expressed relative (1) to siControl. B: Pcyt2 and EGR1 proteins were both dramatically reduced with the siRNA-EGR1 gene silencing under the same conditions as in A. The cells transfected with an unspecific siRNA duplex did not affect the *PCYT2* and EGR1 proteins. C: MCF-7 cells were cultured in MEM containing 10% FBS with insulin and in DMEM/F12 containing 5% horse serum with insulin, epidermal growth factor, and hydrocortisone for 48 h; expression of EGR1 and *PCYT2* was detected with immunoblotting. B, C: An equal amount (25 μg) of protein loading is demonstrated by protein staining with Ponceau S, and duplicate lanes are indicated. Also shown are means ± SD from at least two separate experiments performed in duplicate and expressed relative (1) to the values in MCF-7 cells.

Taken together, we conclude that differences in *PCYT2* gene expression seen in these two cell lines can be attributed to variations in the nuclear activity of the two main regulatory transcription factors, EGR1 and NFκB.

DISCUSSION

Our results, for the first time, demonstrate that the increase in phosphoethanolamine in MCF-7 breast cancer cells could be caused by the downregulation of PE synthesis via the de novo Kennedy pathway at the step of CDP-ethanolamine formation. An increase in the intracellular phosphoethanolamine pool could be attributed to several factors, including the inhibition of its conversion to CDP-ethanolamine via the Kennedy pathway and/or the increase in its formation by ethanolamine phosphorylation and PE degradation (14). Our focus was to understand

the mechanism behind the contribution of the inhibition of the Kennedy pathway, because supportive evidence for the importance of this pathway in the maintenance of the phosphoethanolamine pool in tumor cells has been frequently reported (27–30). For instance, CDP-ethanolamine was usually undetectable in intact tumors by in vivo NMR studies (24), and changes in the phosphoethanolamine pool were often associated with changes in ECT activity but not with the rate of ethanolamine phosphorylation (30). A 10-fold increase above normal phosphoethanolamine levels associated with a low rate of incorporation of [^{14}C]ethanolamine into PE was seen in liver lymphoma (27). In *ras*-transformed mouse fibroblasts, elevations of phosphoethanolamine and phosphocholine pools were partially attributed to the inhibition of the corresponding genes *Pcyt2* and *Pcyt1* (the enzyme catalyzing the conversion of phosphocholine into CDP-choline) (29). Not much is known about how ethanolamine uptake is regulated, but
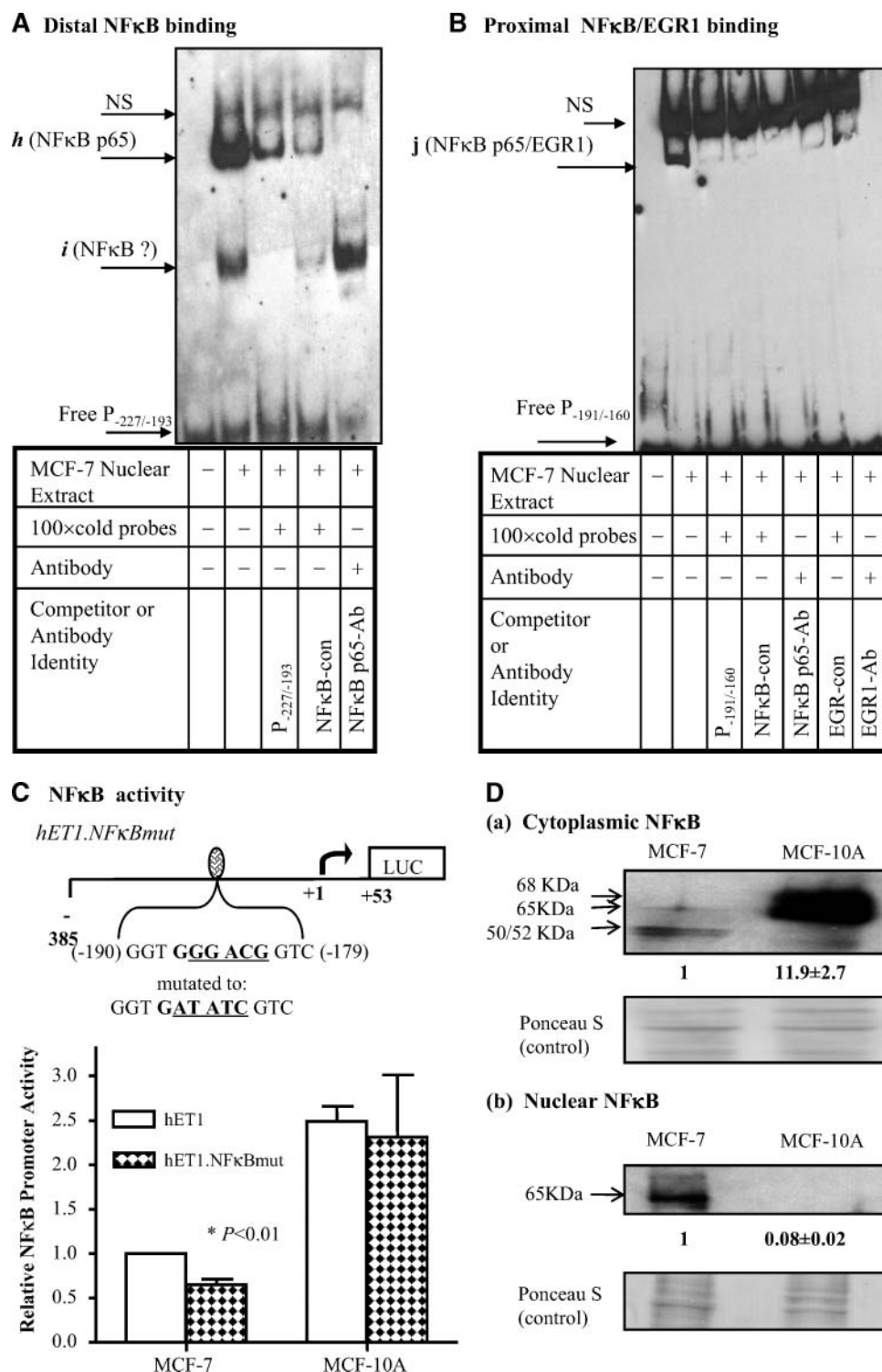
Fig. 8. NFκB binding and activity. A: EMSA with the probe P$_{-227/-193}$ and MCF-7 nuclear extracts. DNA-NFκB complexes were identified by the competition with 100-fold molar excess of "cold" probe, NFκB consensus probe, and p65-specific antibody. B: EMSA analysis of probe P$_{-191/-160}$ with MCF-7 nuclear extracts. The specific interaction was competed for by 100-fold excess of consensus probes and antibodies for NFκB and EGR1. NS indicates nonspecific DNA-protein interactions. The experiments were repeated twice with similar results. C: Diagram of consensus mutation construct LUC.NFκBmut generated from the full-length promoter construct LUC.hET1 (top). Change of LUC.hET1 promoter activity in MCF-7 and MCF-10A cells when an NFκB site ($-187/-182$ bp) was mutated (bottom). *$P < 0.01$. D: Cytoplasmic (20 μg) and nuclear (25 μg) protein levels of NFκB in both cell types were detected by immunoblotting. Numerical data represent mean ± SD from three independent experiments.

Podo (14) postulated that the uptake cannot account for the increase in the phosphoethanolamine pool unless the external substrate concentration is much above its K_t value (i.e., the substrate concentration at half maximal transport activity), which is not the case under most physiological conditions.

Maintaining membrane phospholipid homeostasis is important for normal cell function, and major phospholipid classes are tightly regulated under various metabolic conditions (31, 32). When PE de novo synthesis is limited and PE content is below normal, as in the case of MCF-7 cells, metabolism of other phospholipids, particularly of phosphatidylcholine, is expected to be adjusted accordingly (33). In contrast to PE, it is generally well established that elevated metabolism of PC is present in most cancers (13, 34). An accumulation of the PC metabolite phosphocholine is a result of increased enzyme activities in both biosynthetic and lipolytic pathways, as reported for breast cancers, ovarian tumor cells, and other types of cancer (34). Therefore, it appears reasonable to expect that the PE Kennedy pathway is closely linked with the aberrant PC metabolism in cancers as a necessary event to sustain malignant cell growth and transformation.

Human *PCYT2* gene expression is driven by a GC-rich but TATA-less promoter (9, 15). Transcriptional initiation of a TATA-less promoter usually depends on a proximal CAAT box targeted by NF-Y or C/EBP transcription factors with help from flanking Sp1 binding to a neighboring GC region (35), which is evident in the *PCYT2* promoter, because the CAAT box region is primarily responsible for *PCYT2* transcriptional initiation and this function is shared between the CAAT and GC boxes in both cell types. It is well known that "zinc-finger" transcription factors, such as EGR1 and Sp1, can compete for the same GC-rich promoter regions (36). Putative EGR binding sites within the GC box adjacent to the CAAT box within the *PCYT2* promoter were indicated by a computer database (15). However, EMSA with the probe $P_{-128/-93}$ covering this region did not show any significant binding of EGR1, suggesting that this proximal promoter region has a high affinity for Sp1 proteins as an essential interaction for the basal promoter function. The upregulation of the *PCYT2* promoter in MCF-10A cells is attributed to additional interactions of distal GC-enhancer sites, which were very strongly dependent on EGR1 expression and activity.

Our initial characterization of the human *PCYT2* promoter suggested that both EGR1 and NFκB could be potential regulators of *PCYT2* gene transcription (15). In the current study, we revealed that *PCYT2* gene expression was different in MCF-10A cells and MCF-7 cells that also differ in the expression and nuclear activities of EGR1 and NFκB transcription factors. The role of EGR1 in cancers is not clearly established. In prostate carcinomas, high levels of EGR1 are positively related with tumor growth; however, in other cell types, suppression of growth and transformation has been observed in tumor cells constantly expressing EGR1 (17). EGR1 could suppress the growth and transformation of human fibrosarcoma cells by induction of transforming growth factor β1 (37).

EGR1 also makes complexes with the oncogene c-Jun and activates promoters of the pro-apoptotic genes p53 and PTEN (17). Furthermore, expression of exogenous EGR1 in human breast tumor cells markedly reduced transformed growth and tumorigenicity (38, 39). Wenzel et al. (40) reported that EGR1 expression in MCF-7 cells was associated with an inhibitory protein for type 1 Ser/Thr protein phosphatase, and that the expression of this protein is reduced in breast cancer cells, breast tumors, and metastases. Chemotherapeutic agent-induced EGR1 expression in breast carcinoma cells led to a p53-independent apoptosis (41). However, the mechanisms underlying the loss of EGR1 expression for the dysregulation of normal breast cell growth are not yet fully understood. Our data suggest a novel role for EGR1, to support phospholipid PE synthesis by regulation of *PCYT2* gene expression and by doing this to contribute to membrane phospholipid homeostasis, an essential cellular function commonly perturbed in cancers.

The contribution of NFκB to *PCYT2* gene transcription in normal MCF-10A cells was not significant, because it was overwhelmed by abundant EGR1 activity. In MCF-7 cells, where EGR1 content is significantly lower, NFκB effectively assisted in the regulation of *PCYT2* gene transcription. We found that the significant elevation of NFκB transcriptional activity in MCF-7 cells was caused by increased nuclear translocation of the active subunit RelA (p65). This is in agreement with previous findings established for a panel of breast cancer cells, including MCF-7 cells, which utilize the classical NFκB pathway that targets RelA(p65) nuclear activation (42, 43). All five members of the NFκB family share the 300 amino acid N-terminal Rel homology domain, and the antibody used in this study was raised against 1–286 amino acids containing this domain. It specifically recognized p65 (RelA) and p68 (RelB) subunits but not p75(c-Rel). The breast cancer cells and breast tumors could have a selective upregulation of p50 and p52 expression relative to normal adjacent tissues (43, 44). Our antibody detected a selective increase in the MCF-7 cytoplasmic protein of lower size that could correspond to either p50 or p52 subunits. However, whether there is a different subset of the NFκB subunit activation by different abilities of IκB kinases (IKKα and IKKβ) to phosphorylate IκB in the two cell lines is not known at present and requires further investigation.

NFκB activation is required for normal mammary gland development, and aberrant regulation of NFκB is linked to breast cancer progression (16, 45). The constitutive activation of NFκB is a common marker for a variety of cancers, including breast cancer (16). The activation of NFκB is proposed to facilitate the survival of mutated cells and the growth of tumors, because genetic inactivation of NFκB led to an inhibition of the early stages of tumor development in a mouse model (46). Coincidentally, a relative elevation of ECT activity during the exponential phase of tumor growth was reported (30), suggesting that an active PE synthesis is required for cell growth. In addition, it is worth noting that activation of NFκB occurs frequently in response to radio- and chemotherapy (16). Even though NFκB is thought to be responsible for drug resistance,

drug-induced NFκB activation does not always result in anti-apoptosis, but is required for inducing the activation of pro-apoptotic pathways under some conditions (16, 47). Notably, a decrease in phosphoethanolamine content in response to breast cancer therapy is considered an efficient therapeutic effect (48). Our work is the first to establish a molecular link between NFκB and PE phospholipid metabolism. The relationship between NFκB inactivation and *PCYT2* gene expression in response to cancer therapy will be of interest to explore in the future.

In conclusion, we provide evidence that EGR1 is a critical stimulator of *PCYT2* transcription and that suppression of the *PCYT2* gene could be directly caused by the lower expression of ERG1, as in the MCF-7 breast cancer cells. This work demonstrates that a balance between the abundance and activity of the EGR1 and NFκB transcription factors is critical for the regulation of *PCYT2* gene expression, ultimately controlling the de novo Kennedy pathway for PE synthesis, which, if disrupted, could lead to improper membrane function and signaling, as is frequently observed in various cancers, including breast cancer.▮

REFERENCES

1. Bakovic, M., M. D. Fullerton, and V. Michel. 2007. Metabolic and molecular aspects of ethanolamine phospholipid biosynthesis: the role of CTP:phosphoethanolamine cytidylyltransferase (Pcyt2). *Biochem. Cell Biol.* **85:** 283–300.
2. Emoto, K., T. Kobayashi, A. Yamaji, H. Aizawa, I. Yahara, K. Inoue, and M. Umeda. 1996. Redistribution of phosphatidylethanolamine at the cleavage furrow of dividing cells during cytokinesis. *Proc. Natl. Acad. Sci. USA.* **93:** 12867–12872.
3. Emoto, K., N. Toyama-Sorimachi, H. Karasuyama, K. Inoue, and M. Umeda. 1997. Exposure of phosphatidylethanolamine on the surface of apoptotic cells. *Exp. Cell Res.* **232:** 430–434.
4. Kobayashi, T., and R. E. Pagano. 1989. Lipid transport during mitosis. Alternative pathways for delivery of newly synthesized lipids to the cell surface. *J. Biol. Chem.* **264:** 5966–5973.
5. Kanfer, J. N. 1980. The base exchange enzymes and phospholipase D of mammalian tissue. *Can. J. Biochem.* **58:** 1370–1380.
6. Lee, T. 1998. Biosynthesis and possible biological functions of plasmalogens. *Biochim. Biophys. Acta.* **1394:** 129–145.
7. Sundler, R., and B. Akesson. 1975. Regulation of phospholipid biosynthesis in isolated rat hepatocytes. Effect of different substrates. *J. Biol. Chem.* **250:** 3359–3367.
8. Kennedy, E. P., and S. B. Weiss. 1956. The function of cytidine coenzymes in the biosynthesis of phospholipides. *J. Biol. Chem.* **222:** 193–214.
9. Poloumienko, A., A. Cote, A. T. Quee, L. Zhu, and M. Bakovic. 2004. Genomic organization and differential splicing of the mouse and human Pcyt2 genes. *Gene.* **325:** 145–155.
10. Tie, A., and M. Bakovic. 2007. Alternative splicing of CTP:phosphoethanolamine cytidylyltransferase produces two isoforms that differ in catalytic properties. *J. Lipid Res.* **48:** 2172–2181.
11. Fullerton, M. D., F. Hakimuddin, and M. Bakovic. 2007. Developmental and metabolic effects of disruption of the mouse CTP: phosphoethanolamine cytidylyltransferase gene (Pcyt2). *Mol. Cell. Biol.* **27:** 3327–3336.
12. Orsetti, B., F. Courjal, M. Cuny, C. Rodriguez, and C. Theillet. 1999. 17q21-q25 aberrations in breast cancer: combined allelotyping and CGH analysis reveals 5 regions of allelic imbalance among which two correspond to DNA amplification. *Oncogene.* **18:** 6262–6270.
13. Smith, T. A., C. Bush, C. Jameson, J. C. Titley, M. O. Leach, D. E. Wilman, and V. R. McCready. 1993. Phospholipid metabolites, prognosis and proliferation in human breast carcinoma. *NMR Biomed.* **6:** 318–323.
14. Podo, F. 1999. Tumour phospholipid metabolism. *NMR Biomed.* **12:** 413–439.
15. Johnson, C. M., Z. Yuan, and M. Bakovic. 2005. Characterization of transcription factors and cis-acting elements that regulate human CTP:phosphoethanolamine cytidylyltransferase (Pcyt2). *Biochim. Biophys. Acta.* **1735:** 230–235.
16. Haffner, M. C., C. Berlato, and W. Doppler. 2006. Exploiting our knowledge of NF-kappaB signaling for the treatment of mammary cancer. *J. Mammary Gland Biol. Neoplasia.* **11:** 63–73.
17. Thiel, G., and G. Cibelli. 2002. Regulation of life and death by the zinc finger transcription factor Egr-1. *J. Cell. Physiol.* **193:** 287–292.
18. Huang, R. P., Y. Fan, I. de Belle, C. Niemeyer, M. M. Gottardis, D. Mercola, and E. D. Adamson. 1997. Decreased Egr-1 expression in human, mouse and rat mammary cells and tissues correlates with tumor formation. *Int. J. Cancer.* **72:** 102–109.
19. Bligh, E. G., and W. J. Dyer. 1959. A rapid method of total lipid extraction and purification. *Can. J. Biochem. Physiol.* **37:** 911–917.
20. Porter, T. J., and C. Kent. 1990. Purification and characterization of choline/ethanolamine kinase from rat liver. *J. Biol. Chem.* **265:** 414–422.
21. Zhu, L. J., and S. W. Altmann. 2005. mRNA and 18S-RNA coapplication-reverse transcription for quantitative gene expression analysis. *Anal. Biochem.* **345:** 102–109.
22. Tsai, J. C., L. Liu, J. Zhang, K. C. Spokes, J. N. Topper, and W. C. Aird. 2001. Epidermal growth factor induces Egr-1 promoter activity in hepatocytes in vitro and in vivo. *Am. J. Physiol. Gastrointest. Liver Physiol.* **281:** G1271–G1278.
23. Keeton, A. B., K. D. Bortoff, W. L. Bennett, J. L. Franklin, D. Y. Venable, and J. L. Messina. 2003. Insulin-regulated expression of Egr-1 and Krox20: dependence on ERK1/2 and interaction with p38 and PI3-kinase pathways. *Endocrinology.* **144:** 5402–5410.
24. Hasan, R. N., S. Phukan, and S. Harada. 2003. Differential regulation of early growth response gene-1 expression by insulin and glucose in vascular endothelial cells. *Arterioscler. Thromb. Vasc. Biol.* **23:** 988–993.
25. Revest, J-M., F. Di Blasi, P. Kitchener, F. Rougé-Pont, A. Desmedt, M. Turiault, F. Tronche, and P. V. Piazza. 2005. The MAPK pathway and Egr-1 mediate stress-related behavioral effects of glucocorticoids. *Nat. Neurosci.* **8:** 664–672.
26. Ghosh, S., and M. Karin. 2002. Missing pieces in the NF-kappaB puzzle. *Cell.* **109 (Suppl):** 81–96.
27. Dixon, R. M., and M. Tian. 1993. Phospholipid synthesis in the lymphomatous mouse liver studied by 31P nuclear magnetic resonance spectroscopy in vitro and by administration of 14C-radiolabelled compounds in vivo. *Biochim. Biophys. Acta.* **1181:** 111–121.
28. Franks, S. E., A. C. Kuesel, N. W. Lutz, and W. E. Hull. 1996. 31P MRS of human tumor cells: effects of culture media and conditions on phospholipid metabolite concentrations. *Anticancer Res.* **16:** 1365–1374.
29. Momchilova, A., T. Markovska, and R. Pankov. 1999. Ha-ras-transformation alters the metabolism of phosphatidylethanolamine and phosphatidylcholine in NIH 3T3 fibroblasts. *Cell Biol. Int.* **23:** 603–610.
30. Ronen, S. M., E. Rushkin, and H. Degani. 1992. Lipid metabolism in large T47D human breast cancer spheroids: 31P- and 13C-NMR studies of choline and ethanolamine uptake. *Biochim. Biophys. Acta.* **1138:** 203–212.
31. Li, Z., L. B. Agellon, T. M. Allen, M. Umeda, L. Jewell, A. Mason, and D. E. Vance. 2006. The ratio of phosphatidylcholine to phosphatidylethanolamine influences membrane integrity and steatohepatitis. *Cell Metab.* **3:** 321–331.
32. Steenbergen, R., T. S. Nanowski, R. Nelson, S. G. Young, and J. E. Vance. 2006. Phospholipid homeostasis in phosphatidylserine synthase-2-deficient mice. *Biochim. Biophys. Acta.* **1761:** 313–323.
33. Zhang, R., L. Barker, D. Pinchev, J. Marshall, M. Rasamoelisolo, C. Smith, P. Kupchak, I. Kireeva, L. Ingratta, and G. Jackowski. 2004. Mining biomarkers in human sera using proteomic tools. *Proteomics.* **4:** 244–256.
34. Iorio, E., D. Mezzanzanica, P. Alberti, F. Spadaro, C. Ramoni, S. D'Ascenzo, D. Millimaggi, A. Pavan, V. Dolo, S. Canevari, et al. 2005. Alterations of choline phospholipid metabolism in ovarian tumor progression. *Cancer Res.* **65:** 9369–9376.
35. Bolognese, F., M. Pitarque-Marti, V. Lo Cicero, R. Mantovani, and J. A. Maier. 2006. Characterization of the human EDF-1 minimal promoter: involvement of NFY and Sp1 in the regulation of basal transcription. *Gene.* **374:** 87–95.
36. Khachigian, L. M., V. Lindner, A. J. Williams, and T. Collins. 1996. Egr-1-induced endothelial gene expression: a common theme in vascular injury. *Science.* **271:** 1427–1431.

ASBMB

JOURNAL OF LIPID RESEARCH

37. Liu, C., E. Adamson, and D. Mercola. 1996. Transcription factor EGR-1 suppresses the growth and transformation of human HT-1080 fibrosarcoma cells by induction of transforming growth factor beta 1. *Proc. Natl. Acad. Sci. USA.* **93:** 11831–11836.

38. Huang, R. P., T. Darland, D. Okamura, D. Mercola, and E. D. Adamson. 1994. Suppression of v-sis-dependent transformation by the transcription factor, Egr-1. *Oncogene.* **9:** 1367–1377.

39. Huang, R. P., C. Liu, Y. Fan, D. Mercola, and E. D. Adamson. 1995. Egr-1 negatively regulates human tumor cell growth via the DNA-binding domain. *Cancer Res.* **55:** 5054–5062.

40. Wenzel, K., K. Daskalow, F. Herse, S. Seitz, U. Zacharias, J. A. Schenk, H. Schulz, N. Hubner, B. Micheel, P. M. Schlag, et al. 2007. Expression of the protein phosphatase 1 inhibitor KEPI is downregulated in breast cancer cell lines and tissues and involved in the regulation of the tumor suppressor EGR1 via the MEK-ERK pathway. *Biol. Chem.* **388:** 489–495.

41. Kim, C. G., B. H. Choi, S. W. Son, S. J. Yi, S. Y. Shin, and Y. H. Lee. 2007. Tamoxifen-induced activation of p21Waf1/Cip1 gene transcription is mediated by Early Growth Response-1 protein through the JNK and p38 MAP kinase/Elk-1 cascades in MDA-MB-361 breast carcinoma cells. *Cell. Signal.* **19:** 1290–1300.

42. Lee, C. H., Y-T. Jeon, S-H. Kim, and Y-S. Song. 2007. NF-kappaB as a potential molecular target for cancer therapy. *Biofactors.* **29:** 19–35.

43. Cogswell, P. C., D. C. Guttridge, W. K. Funkhouser, and A. S. Baldwin, Jr. 2000. Selective activation of NF-kappaB subunits in human breast cancer: potential roles for NF-kappaB2/p52 and for Bcl-3. *Oncogene.* **19:** 1123–1131.

44. Zhou, Y., S. Eppenberger-Castori, C. Marx, C. Yau, G. K. Scott, U. Eppenberger, and C. C. Benz. 2005. Activation of nuclear factor-κB (NFκB) identifies a high-risk subset of hormone-dependent breast cancers. *Int. J. Biochem. Cell Biol.* **37:** 1130–1144.

45. Geymayer, S., and W. Doppler. 2000. Activation of NF-kappaB p50/p65 is regulated in the developing mammary gland and inhibits STAT5-mediated beta-casein gene expression. *FASEB J.* **14:** 1159–1170.

46. Greten, F. R., L. Eckmann, T. F. Greten, J. M. Park, Z. W. Li, L. J. Egan, M. F. Kagnoff, and M. Karin. 2004. IKKbeta links inflammation and tumorigenesis in a mouse model of colitis-associated cancer. *Cell.* **118:** 285–296.

47. Farhana, L., M. I. Dawson, and J. A. Fontana. 2005. Apoptosis induction by a novel retinoid-related molecule requires nuclear factor-kappaB activation. *Cancer Res.* **65:** 4909–4917.

48. Ng, T. C., S. Grundfest, S. Vijayakumar, N. J. Baldwin, A. W. Majors, I. Karalis, T. F. Meaney, K. H. Shin, F. J. Thomas, and R. Tubbs. 1989. Therapeutic response of breast carcinoma monitored by 31P MRS in situ. *Magn. Reson. Med.* **10:** 125–134.